ORIGINAL ARTICLE

Realizing 32-time Scan Duration Reduction of ^{18}F-FDG PET Using Deep Learning Model with Image Augmentation

Ali Ghafari [1], Peyman Sheikhzadeh [1, 2*], Negisa Seyyedi [3], Mehrshad Abbasi [2], Mohammad Reza Ay [1, 4]

[1] Department of Medical Physics and Biomedical Engineering, School of Medicine, Tehran University of Medical Sciences, Tehran, Iran

[2] Department of Nuclear Medicine, Imam Khomeini Hospital Complex, Tehran University of Medical Sciences, Tehran, Iran

[3] Nursing and Midwifery Care Research Center, Iran University of Medical Sciences, Tehran, Iran

[4] Research Center for Molecular and Cellular Imaging, Tehran University of Medical Sciences, Tehran, Iran

*Corresponding Author: Peyman Sheikhzadeh
Email: sheikhzadeh-p@sina.tums.ac.ir

Received: 18 May 2022 / Accepted: 17 July 2022

Abstract

Purpose: 32-time scan duration reduction of ^{18}F-Fluorodeoxyglucose (^{18}F-FDG) Positron Emission Tomography (PET) images through the generation of standard scan duration images using a multi-slice cycle-consistent Generative Adversarial Network (cycle-GAN) was studied. Also, the effect of the image augmentation methods on the performance of the cycle-GAN model was evaluated.

Materials and Methods: Four subsets of standard and 32-time short scan duration PET image pairs, each contacting image data of 10 patients were used to train and test (80 percent for training and 20 percent for testing) a multi-slice cycle-GAN separately. Another patient's image data was used as the validation dataset for different training subsets. When training the cycle-GAN model for each subset, two approaches were followed: with and without image augmentation. Common image quality metrics of Peak Signal-to-Noise Ratio (PSNR), Structural Similarity Index Measure (SSIM), and Normalized Root Mean Squared Error (NRMSE) were used to assess the generation performance of the cycle-GAN model. Paired sample t-test statistical testing with a confidence interval of 0.95 was used to determine whether the differences between approaches were statistically significant or not.

Results: For subsets 1-3, both training approaches improved the image quality of the short scan duration inputs ($p < 0.001$) while for subset 4 only the training approach with image augmentation was capable of improving the image quality. However, the training approach with image augmentation offered better results than the approach without image augmentation ($p < 0.001$).

Conclusion: Employing the training approach with image augmentation, the cycle-GAN model was capable of improving the image quality of 1/32nd short scan duration images through the generation of synthetic standard scan duration images. In the case of the training approach without image augmentation, except for subset 4, the model trained on all subsets 1-3 was capable of improving the image quality. Image augmentation does indeed improve the performance of the cycle-GAN model, especially in the case of insufficient available training datasets.

Keywords: Image Augmentation; ^{18}F-Fluorodeoxyglucose; Positron Emission Tomography; Deep Learning.

DOI: https://doi.org/10.18502/fbt.v10i2.12224

Frontiers in BIOMEDICAL TECHNOLOGIES

1. Introduction

Positron Emission Tomography (PET) modality provides semi-quantitative and functional data and has multiple applications in different subjects of medicine [1-4]. Positron Emission Tomography / Computed Tomography (PET/CT) is an extended modality compared to stand-alone PET used for various purposes, including diagnosis and prognosis since it has the added capability of providing fine anatomical structural information [5, 6]. Image quality, cost-efficiency, and radiation safety considerations of PET imaging are affected by the scan duration or radiotracer dosage [4]. Imaging department throughput and patient comfort are affected by the scan duration while radiation dose and scan cost are controlled by the radiotracer dosage [4]. There are sensible reasons for decreasing the scan duration or radiotracer injected dose since it addresses important matters, including the cost of imaging and addressing radiation safety considerations. However, it comes at the cost of much more noise in the images with a subsequent decrease in the accuracy of diagnosis [4, 7, 8].

Deep learning methods have found their role in the medical imaging field, including diagnosis [9], image post-processing, and restoration by performing operations like denoising [10 - 21]. Generative Adversarial Networks (GANs) are deep learning models learning to capture the distribution of data [22]. GANs are typically composed of a generator and discriminator network training to outperform the other network in an adversarial manner. The generator intends to generate more realistic images to deceive the discriminator network to label the synthetic images as real ones [22]. On the other hand, the discriminator network tries to improve its classification accuracy to not misclassify synthetic or generated images as real ones [4, 22-23].

Multiple previous studies have attempted to generate standard dose/scan duration images from various inputs [4, 16, 21, 24-28] and achieved notable results. Xue *et al.* [4] implemented a mapping between low-count sinogram data to full-count PET images using a GAN framework. As stated by the authors [1], their implementation had the advantage of faster reconstruction speed compared to iterative methods and the capability of direct reconstruction of the full-count images from low-count sinogram inputs. Zhao *et al.* [21], to restore low-dose Brain PET images, developed the S-cycleGAN to achieve a non-linear and end-to-end mapping. They [21] used the cycle-consistency loss, Wasserstein distance, and supervised learning loss in their model. They [21] reported high accuracy and appropriate efficiency of their model using the quantitative evaluation of metrics like Peak Signal-to-Noise Ratio (PSNR). Wang *et al.* [27] used a Convolutional Neural Network (CNN) to predict ^{18}F-Fluorodeoxyglucose (^{18}F-FDG) PET images using the 6.25% simulated low-dose inputs. Ouyang *et al.* [25] used a GAN along with feature matching and task-specific perceptual loss specific to generate amyloid PET images with standard-dose using only low-dose PET. In this study, 40 PET datasets were obtained from 39 patients using a PET/MR scanner. The two-dimensional encoder-decoder network has been used as a generator to produce standard-dose images and a discriminator to evaluate them. The quality of the image was evaluated using the PSNR, the Structural Similarity index (SSIM) and the Root Mean Square Error (RMSE). Finally, the authors concluded that standard-dose PET images of amyloid can be produced using very low-dose images. Also, it is necessary to apply adversarial learning, feature matching, and task-specific perceptual loss to ensure image quality and maintain pathological features. Lei *et al.* [29] studied the possibility of reducing scan time or injected radiotracer activity in PET imaging and solving the subsequent problem of low-count statistics using a cycle-consistent GAN model. They proposed this model to estimate PET images with diagnostic quality from low count data. The authors were able to develop a deep learning-based procedure that can correctly estimate PET data with diagnostic quality from 1/8th fraction of standard photon counts having great potential for improving low-count PET image quality.

However, little or no effort has been made to clarify the effect of image augmentation in the process of image generation since providing enough data to train the generative model is a challenge and it is not always feasible to acquire a large amount of data for training due to different considerations, including costs of imaging and radiation hazards. This matter of low available training data can be addressed using image augmentation techniques that increase the variability of data available.

In this study, we aim to assess the effect of image augmentation on the performance of the cycle-GAN model generating standard scan duration ^{18}F-FDG PET images using the 1/32nd short scan duration inputs for four different subsets of data.

The rest of this paper is organized as follows: Section 2 provides details about the materials and methods used in

the study. Section 3 reports the results that are discussed in Section 4. Section 5 concludes the study and states the possible future extension to this study.

2. Materials and Methods

2.1. Materials

Using a PET/CT scanner (5-ring BGO-based GE discovery-IQ), whole-body PET scans of 41 patients were acquired using a standard 18F-FDG radioactivity dose of 294.52 ± 45.18 MBq. Image data were reconstructed using Ordered-Subset Expectation Maximization (OSEM) (four iterations and 12 subsets). 1/32nd short scan duration image data of the patients were acquired through post-reconstruction of the image data using the same reconstruction settings but with only 1/32nd scan duration for each bed position.

A patient was randomly assigned as the validation dataset and the remaining 40 patients were randomly divided into 4 subsets (subsets 1 through 4) to explore the effects of image augmentation and generation performance. More detailed information about the subsets is present in Table 1. For each subset, image data of eight patients were used for training the multi-slice cycle-consistent generative adversarial network (cycle-GAN) and the image data of the two remaining patients were used for testing the performance of the cycle-GAN.

2.2. Methods

2.2.1. Image Generation

GANs are used for image generation using a mapping learned from input-target pairs or data distributions. In this study, a cycle-GAN is used for style transfer or mapping between short scan duration images (referred to as shortSD) as input and standard scan duration images (referred to as StandardSD) as targets. Cycle-GAN offers better performance over simple GAN and mostly has overcome previous GAN types problems [4, 30, 31]. Cycle-GAN has two generator and discriminator network pairs (one for short to standard scan duration generation and one in the reverse direction). The generator generates synthetic images and the discriminator tries to differentiate between synthetic and original images. Both generator and discriminator try to improve their performance leading to the overall improved performance of the cycle-GAN network. The image dimensions are (192, 192) and the three following slices are stacked together in to provide multi-slice input to the cycle-GAN network and decrease the training time. The ADAM optimizer with a learning rate of 0.0002 was used to optimize the models. More detail about the generator and discriminator models' structure is provided in Figures 1 and 2.

2.2.2. Implementation Process

We followed two approaches when training the cycle-GAN model for each subset: first, training the cycle-GAN for 250 epochs Without Image Augmentation (WoIA). Second, training the cycle-GAN With Image Augmentation for 250 epochs (WIA). In this study, image augmentation is achieved through methods that do not alter the pixel values of the images for the simplicity and consistency between short and standard scan duration image counterparts. Before each epoch, all Image pairs (short scan duration and standard scan duration) go through the following process of image augmentation. All augmentations steps were done randomly:

Table 1. Detailed information about the data used in this study

Subsets		Standard Scan Duration (s)	Activity (MBq)	Number of slices
Subset 1	Train	541.25 ± 87.66	267.6 ± 3.54.96	2808
	Test	570 ± 77	285.83 ± 50.88	702
Subset 2	Train	660.63 ± 84.15	328.34 ± 48.18	2937
	Test	675 ± 35	311.45 ± 28.21	768
Subset 3	Train	570 ± 89.24	286.11 ± 45.53	2871
	Test	780 ± 130	301.33 ± 18.72	768
Subset 4	Train	622.5 ± 46.21	301.13 ± 22	2778
	Test	620 ± 30	264 ± 11.28	702
Validation		570	284.9	351

$Up\ and\ down\ flip \rightarrow Left\ and\ right\ flip \rightarrow Multiples\ of\ 45\ degree\ rotation\ (0, 45, 90, and\ 135\ degrees)$

2.2.3. Performance Evaluation Metrics

The performance of the cycle-GAN model on different subsets (with and without augmentation) was evaluated using the PSNR, SSIM [32] and Normalized Root Mean Squared Error (NRMSE) (Equations 1-3). PSNR measures the noise level of the test images (short scan duration and synthetic standard scan duration) compared to the ground truth images (standard scan duration). SSIM measures the similarity of structures present in the two images (short and synthetic standard scan duration compared to original standard scan duration). NRMSE is also a measure of the error between test and standard scan duration images.

$$PSNR = 10\ \log_{10}\left(\frac{MAX^2}{\frac{1}{n}\sum_{i=1}^{n}(T_i - I_i)^2}\right) \quad (1)$$

$$SSIM = \frac{(2\mu_T\mu_I + C_1)(2\sigma_{TI} + C_2)}{({\mu_T}^2 + {\mu_I}^2 + C_1)({\sigma_T}^2 + {\sigma_I}^2 + C_2)} \quad (2)$$

$$NRMSE = \sqrt{\sum_{i=1}^{n}\frac{(T-I)^2}{n}} \quad (3)$$

In Equations 1-3, μ, and σ stand for mean and variance. Also, T, I, n, and MAX denote original value, predicted value, number of pixels, and maximum pixel value. C1 and C2 are constants used in the calculation of the SSIM. To determine whether the difference between synthesized (generated) standard scan duration and original standard scan duration images (ground truth used for calculation of metrics) in terms of PSNR, SSIM, and NRMSE metrics are statistically significant, we used the paired-sample t-test with a confident interval of 0.95.

3. Results

For all subsets of data, both training approaches (with and without augmentation) of the cycle-GAN model were capable of improving the image quality evaluation metrics i.e., PSNR, SSIM, NRMSE. The paired sample t-test statistical testing was performed with a confidence interval of %95 to determine whether the difference between the results was statistically significant. Table 2 presents the results of the cycle-GAN model for all subsets and both training approaches. Differences between all results were proved to be statistically significant ($p < 0.001$). Although both approaches lead to quality improvement of the short scan duration images, however, training the cycle-

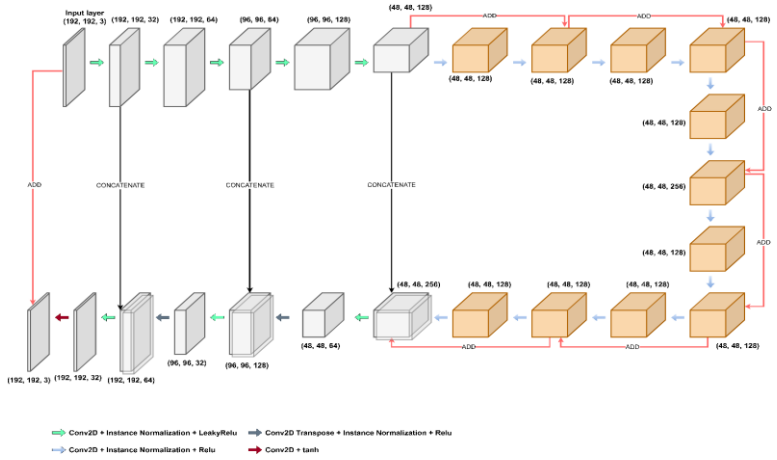

Figure 1. The structure of the U-shaped generator network has Add and Concatenate skip connection to preserve the structural details as the network deepens

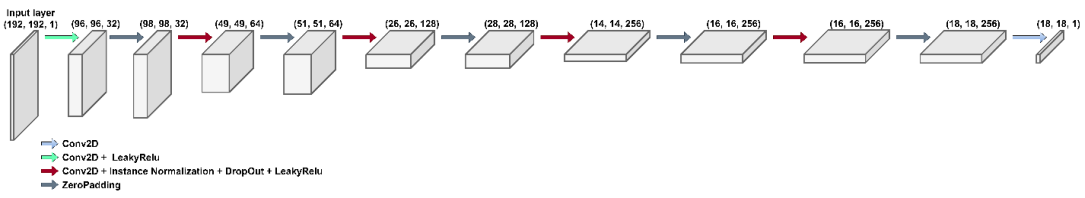

Figure 2. The structure of the discriminator network

GAN model with the image augmentation approach leads to better performance of the model.

Exploring the performance of the model after each training epoch can provide useful insight into the effects of image augmentation. For this purpose, we analyzed the performance of the cycle-GAN model trained using different training subsets on a separate subset of patient image data (validation subset) to observe the changes in the metric values. Figures 3-5 plots the value changes of the PSNR, SSIM, and NRMSE metrics during the training process for all four subsets.

Table 2. Results of the standard scan duration PET image generation using the 1/32nd short scan duration input on test data of each training subset

Subset	PSNR[a]			SSIM[b]			NRMSE[c]		
	shortSD[d]	sStandardSD[e] (WoIA[f])	sStandardSD (WIA[g])	shortSD	sStandardSD (WoIA)	sStandardSD (WIA)	shortSD	sStandardSD (WoIA)	sStandardSD (WIA)
1	27.8770	30.8170	31.1178	0.929116	0.943015	0.944623	0.049078	0.032113	0.031690
2	26.2693	30.2898	30.4851	0.927221	0.944137	0.945881	0.053920	0.032654	0.032487
3	26.340558	29.119623	30.040367	0.920549	0.930521	0.937733	0.054980	0.036639	0.033876
4	27.914110	27.914252	31.625818	0.934889	0.934889	0.951590	0.046740	0.046739	0.028404

a: Peak signal-to-noise ratio with the standard scan duration images as ground truth. b: Structural similarity index regarding the standard scan duration images. c: Normalized root means squared error. d: Short scan duration. e: Synthetic standard scan duration. f: Training approach without image augmentation. g: Training approach with image augmentation

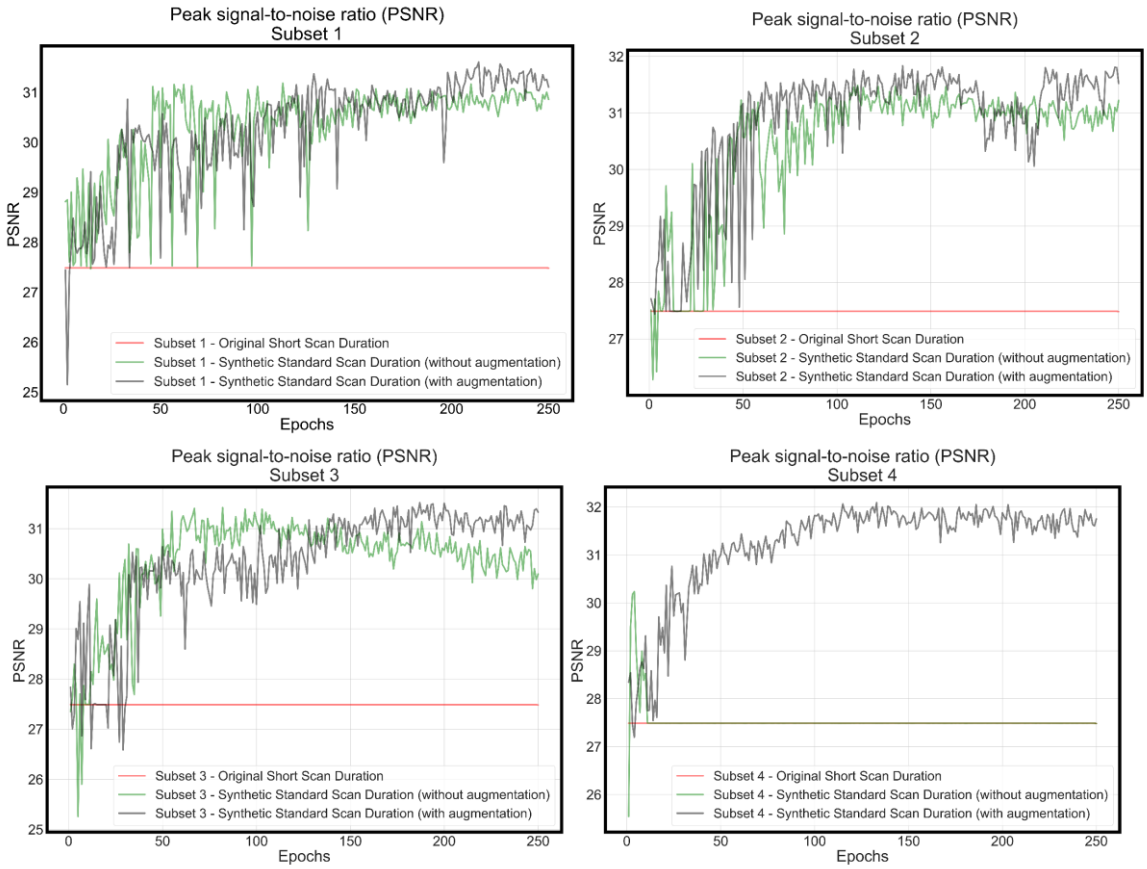

Figure 3. Changes of the PSNR metrics with the increasing training epochs number for both training approaches (with and without augmentation) for all four subsets

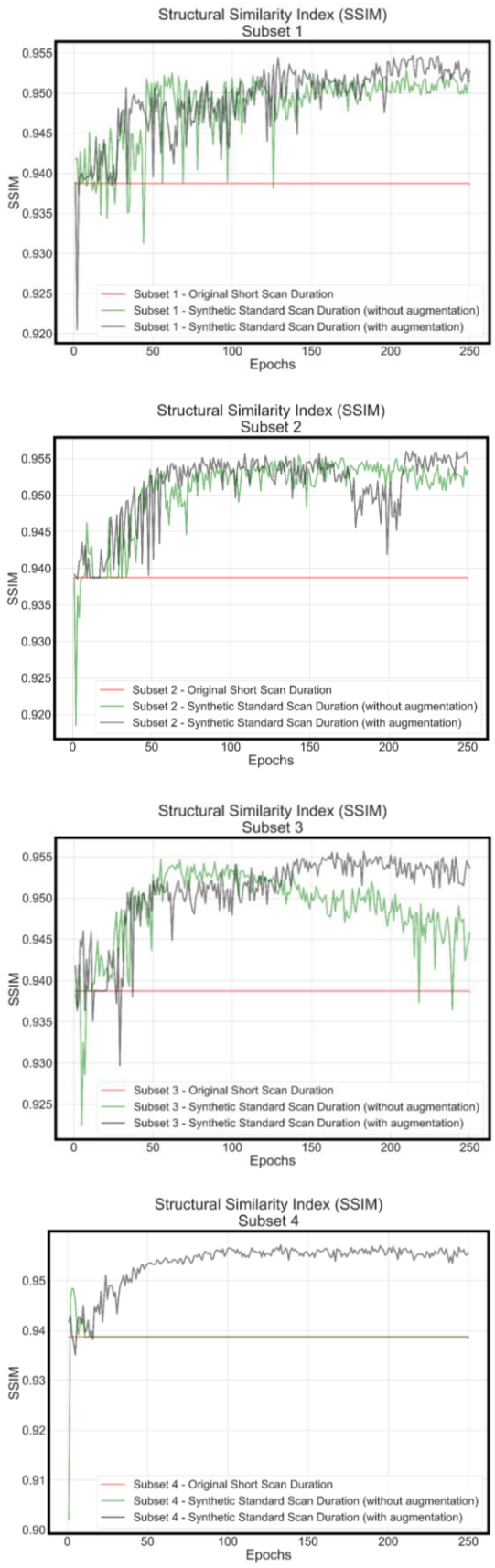

Figure 4. Changes of the SSIM metrics with the increasing training epochs number for both training approaches (with and without augmentation) for all four subsets

4. Discussion

Using a multi-slice input cycle-GAN, we synthesized standard scan duration PET images. Synthetic image quality was improved compared to the short scan duration inputs in terms of PSNR, SSIM, and NRMSE metrics for all four subsets using image augmentation approaches. In the case of the training approach without image augmentation, except for subset 4, all of the other subsets experience improvement in considering the PSNR, SSIM, and NRMSE metrics. Table 2 reports the results of the PSNR, SSIM, and NRMSE metrics for all four subsets in the case of training approaches with and without augmentation (WIA and WoIA, respectively). WIA approach provided statistically and significantly better results than the WoIA approach, especially in the case of subset 4 where the WoIA approach failed to improve the image quality of the short scan duration inputs while the WIA approach yielded better results consistent with the other subsets (1-3). The model trained on the subset 4 dataset using the without image augmentation training approach collapsed and could not synthesize standard scan duration PET images; whereas, the model trained using the training approach with image augmentation approach provided a notable outcome. Also, this could be considered as another merit to image augmentation which is to prevent models from collapsing.

Figures 3-5 plot the curves of the PSNR, SSIM, and NRMSE metrics calculated after each epoch of training for all subsets and both training approaches. It is noticeable that the model trained using the approach with image augmentation keeps on improving as the training epoch increases and surpasses the model trained using the approach without image augmentation.

Image augmentation techniques used in this study, i.e., random up-and-down flip, random left-and-right flip, and multiple 45-degree rotations were all basic image augmentation techniques compared to much more advanced techniques. It was shown that image augmentation techniques do improve the image generation performance of the generative models, including the cycle-GAN model, especially in the case of standard scan duration PET image generation that could be extended to other applications as well. However, more complicated and sophisticated image augmentation techniques should be adopted and evaluated as the techniques employed in this study did not alter the pixel values of the images.

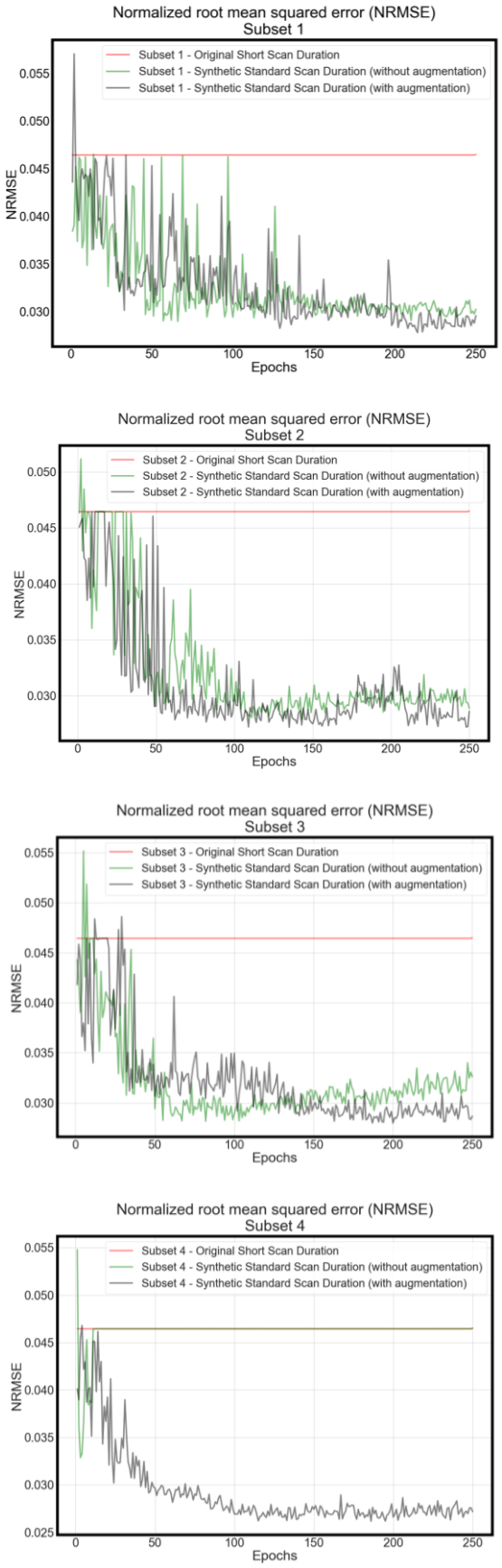

Figure 5. Changes of the NRMSE metrics with the increasing training epochs number for both training approaches (with and without augmentation) for all four subsets

Xu *et al.* [4] evaluated the PSNR, SSIM, and NRMSE metrics. Using raw list-mode count data and 0.5% resampling, 200-time low-dose data were acquired which is so much lower than the 32-time lower scan duration data used in this study. They reported a 19.395%, 7%, and 73.75% improvement of two selected slices of the brain regarding the PSNR, SSIM, and NRMSE metrics. However, in our study using the without image augmentation method, PSNR, SSIM, and NRMSE improved on average for all subsets by about 9.101%, 1.101%, and 26.842%, respectively. The image augmentation approach did improve the performance with 13.754%, 1.834, and 38.198% improvement of the PSNR, SSIM, and NRMSE metrics, respectively. Although the results of the study implemented by the Xu *et al.* [4] are better, their study was dedicated to the brain region while our study was using whole-body data. Zhao *et al.* [21] used 10% and 30% of the original counts as the low-dose inputs. They also measured the PSNR, SSIM, and NRMSE metrics. Excluding the PSNR, which experienced a 0.824% and 0.034% decrease for 10% and 30% low-dose inputs, the SSIM improved by 1.975% and 0.303% for 10% and 30% low-dose inputs. The NRMSE metrics were also improved by 31.4% and 14.84% for 10% and 30% low-dose inputs. Our study, with much fewer data and using the whole-body data, compared to brain data used by Zhao *et al.* [21], offered better results. Although some studies had better results, however, to the best of our knowledge, the effect of image augmentation on the performance of the standard scan duration or standard-dose PET images is not evaluated in related works.

The following study has multiple advantages and disadvantages. Few studies have explored the 32-time reduction in scan duration or injected radiopharmaceutical. Also, exploring the effect of image augmentation on the performance of deep learning models for the task of generating standard scan duration or standard-dose PET images is scarce. We evaluated the performance of our model with and without image augmentation approaches for four different subsets. Nonetheless, there are shortcomings to this study. It would be better to have more patient data in each training subset to have a more comprehensive evaluation. Much more advanced image augmentation methods should be explored to determine the difference in the performance of image augmentation methods in this specific task.

5. Conclusion

In this study, we trained a multi-slice cycle-GAN using four subsets of 1/32nd short scan duration and standard scan duration PET image pairs using two training approaches: with and without image augmentation. Both approaches improved the image quality of the short scan duration inputs. However, models trained using the image augmentation approach offered statistically significant and better results than those without the image augmentation approach. Image augmentation proves to be useful when a more comprehensive dataset is not available for applications like the generation of synthetic standard scan duration PET image of this study. A more comprehensive study should also be conducted about other more advanced and sophisticated techniques of image augmentation.

Acknowledgments

This study was funded by the Tehran University of Medical Sciences [Grant Number 49551].

References

1- Thomas Beyer *et al.*, "A combined PET/CT scanner for clinical oncology." *Journal of nuclear medicine*, Vol. 41 (No. 8), pp. 1369-79, (2000).

2- Roger N Gunn, Mark Slifstein, Graham E Searle, and Julie C Price, "Quantitative imaging of protein targets in the human brain with PET." *Physics in Medicine & Biology*, Vol. 60 (No. 22), p. R363, (2015).

3- Josef Machac, "Cardiac positron emission tomography imaging." in *Seminars in nuclear medicine*, (2005), Vol. 35 (No. 1): *Elsevier*, pp. 17-36.

4- Hengzhi Xue *et al.*, "LCPR-Net: low-count PET image reconstruction using the domain transform and cycle-consistent generative adversarial networks." *Quantitative Imaging in Medicine and Surgery*, Vol. 11 (No. 2), p. 749, (2021).

5- Junichi Tsuchiya *et al.*, "Deep learning-based image quality improvement of 18F-fluorodeoxyglucose positron emission tomography: a retrospective observational study." *EJNMMI physics*, Vol. 8 (No. 1), pp. 1-12, (2021).

6- Richard L. Wagner Henry N. Ovid Technologies Inc Wahl, "Principles and practice of PET and PET/CT." (in English), (2009).

7- Nicolas A Karakatsanis, Eleni Fokou, and Charalampos Tsoumpas, "Dosage optimization in positron emission tomography: state-of-the-art methods and future prospects." *American journal of nuclear medicine and molecular imaging*, Vol. 5 (No. 5), p. 527, (2015).

8- Soo Mee Kim, Adam M Alessio, Bruno De Man, and Paul E Kinahan, "Direct Reconstruction of CT-Based Attenuation Correction Images for PET With Cluster-Based Penalties." *IEEE transactions on nuclear science*, Vol. 64 (No. 3), pp. 959-68, (2017).

9- Azar Amir Sorayaie *et al.*, "Covidense: Providing a Suitable Solution for Diagnosing Covid-19 Lung Infection Based on Deep Learning from Chest X-Ray Images of Patients." (2021).

10- Motonori Akagi *et al.*, "Deep learning reconstruction improves image quality of abdominal ultra-high-resolution CT." *European radiology*, Vol. 29 (No. 11), pp. 6163-71, (2019).

11- Kuang Gong, Jiahui Guan, Chih-Chieh Liu, and Jinyi Qi, "PET image denoising using a deep neural network through fine tuning." *IEEE Transactions on Radiation and Plasma Medical Sciences*, Vol. 3 (No. 2), pp. 153-61, (2018).

12- Andreas Hauptmann, Simon Arridge, Felix Lucka, Vivek Muthurangu, and Jennifer A Steeden, "Real-time cardiovascular MR with spatio-temporal artifact suppression using deep learning–proof of concept in congenital heart disease." *Magnetic resonance in medicine*, Vol. 81 (No. 2), pp. 1143-56, (2019).

13- Zhanli Hu *et al.*, "Obtaining PET/CT images from non-attenuation corrected PET images in a single PET system using Wasserstein generative adversarial networks." *Physics in Medicine & Biology*, Vol. 65 (No. 21), p. 215010, (2020).

14- Zhanli Hu *et al.*, "DPIR-Net: Direct PET image reconstruction based on the Wasserstein generative adversarial network." *IEEE Transactions on Radiation and Plasma Medical Sciences*, Vol. 5 (No. 1), pp. 35-43, (2020).

15- Masafumi Kidoh *et al.*, "Deep learning based noise reduction for brain MR imaging: tests on phantoms and healthy volunteers." *Magnetic Resonance in Medical Sciences*, Vol. 19 (No. 3), p. 195, (2020).

16- Juan Liu, Masoud Malekzadeh, Niloufar Mirian, Tzu-An Song, Chi Liu, and Joyita Dutta, "Artificial intelligence-based image enhancement in pet imaging: Noise reduction and resolution enhancement." *PET clinics*, Vol. 16 (No. 4), pp. 553-76, (2021).

17- Fuminari Tatsugami *et al.*, "Deep learning–based image restoration algorithm for coronary CT angiography." *European radiology*, Vol. 29 (No. 10), pp. 5322-29, (2019).

18- Ge Wang, "A perspective on deep imaging." *IEEE access*, Vol. 4pp. 8914-24, (2016).

19- Junshen Xu, Enhao Gong, John Pauly, and Greg Zaharchuk, "200x low-dose PET reconstruction using deep learning." *arXiv preprint arXiv:1712.04119*, (2017).

20- Qiyang Zhang *et al.*, "PET image reconstruction using a cascading back-projection neural network." *IEEE Journal of Selected Topics in Signal Processing*, Vol. 14 (No. 6), pp. 1100-11, (2020).

21- Kui Zhao *et al.*, "Study of low-dose PET image recovery using supervised learning with CycleGAN." *Plos one*, Vol. 15 (No. 9), p. e0238455, (2020).

22- Ian Goodfellow *et al.*, "Generative adversarial nets." *Advances in neural information processing systems*, Vol. 27(2014).

23- Jyoti Islam and Yanqing Zhang, "GAN-based synthetic brain PET image generation." *Brain informatics*, Vol. 7 (No. 1), pp. 1-12, (2020).

24- Young Jin Jeong *et al.*, "Restoration of amyloid PET images obtained with short-time data using a generative adversarial networks framework." *Scientific reports*, Vol. 11 (No. 1), pp. 1-11, (2021).

25- Jiahong Ouyang, Kevin T Chen, Enhao Gong, John Pauly, and Greg Zaharchuk, "Ultra-low-dose PET reconstruction using generative adversarial network with feature matching and task-specific perceptual loss." *Medical physics*, Vol. 46 (No. 8), pp. 3555-64, (2019).

26- Amirhossein Sanaat, Isaac Shiri, Hossein Arabi, Ismini Mainta, René Nkoulou, and Habib Zaidi, "Deep learning-assisted ultra-fast/low-dose whole-body PET/CT imaging." *European journal of nuclear medicine and molecular imaging*, Vol. 48 (No. 8), pp. 2405-15, (2021).

27- Yan-Ran Joyce Wang *et al.*, "Artificial intelligence enables whole-body positron emission tomography scans with minimal radiation exposure." *European journal of nuclear medicine and molecular imaging*, Vol. 48 (No. 9), pp. 2771-81, (2021).

28- Long Zhou, Joshua D Schaefferkoetter, Ivan WK Tham, Gang Huang, and Jianhua Yan, "Supervised learning with cyclegan for low-dose FDG PET image denoising." *Medical image analysis*, Vol. 65p. 101770, (2020).

29- Yang Lei *et al.*, "Whole-body PET estimation from low count statistics using cycle-consistent generative adversarial networks." *Physics in Medicine & Biology*, Vol. 64 (No. 21), p. 215017, (2019).

30- Eunhee Kang, Hyun Jung Koo, Dong Hyun Yang, Joon Bum Seo, and Jong Chul Ye, "Cycle-consistent adversarial denoising network for multiphase coronary CT angiography." *Medical physics*, Vol. 46 (No. 2), pp. 550-62, (2019).

31- Jun-Yan Zhu, Taesung Park, Phillip Isola, and Alexei A Efros, "Unpaired image-to-image translation using cycle-consistent adversarial networks." in *Proceedings of the IEEE international conference on computer vision*, (2017), pp. 2223-32.

32- Zhou Wang, Alan C Bovik, Hamid R Sheikh, and Eero P Simoncelli, "Image quality assessment: from error measurement to structural similarity." *IEEE transactions on image processing*, Vol. 13 (No. 1), (2004).